Cement and Concrete Research 41 (2011) 1339–1348

Contents lists available at ScienceDirect

Cement and Concrete Research

journal homepage: http://ees.elsevier.com/CEMCON/default.asp

Accelerated growth of calcium silicate hydrates: Experiments and simulations

Luc Nicoleau *

BASF Construction Chemicals GmbH, Global Research Polymers for Inorganics, 32 Albert Frank Straße, D-83308 Trostberg, Germany

ARTICLE INFO

Article history:
Received 1 November 2010
Accepted 21 April 2011

Keywords:
C–S–H
Alite
Acceleration
Hydration
SEM

ABSTRACT

Despite the usefulness of isothermal calorimetry in cement analytics, without any further computations this brings only little information on the nucleation and growth of hydrates. A model originally developed by Garrault et al. is used in this study in order to simulate hydration curves of cement obtained by calorimetry with different known hardening accelerators. The limited basis set of parameters used in this model, having a physical or chemical significance, is valuable for a better understanding of mechanisms underlying in the acceleration of C–S–H precipitation. Alite hydration in presence of four different types of hardening accelerators was investigated. It is evidenced that each accelerator type plays a specific role on one or several growth parameters and that the model may support the development of new accelerators. Those simulations supported by experimental observations enable us to follow the formation of the C–S–H layer around grains and to extract interesting information on its apparent permeability.

1. Introduction

Due to necessities to minimize the energy consumption and to have faster construction processes worldwide, the cement portion of next generation concretes must be significantly reduced and has to react more rapidly. For this reason, the concrete producer requires efficient hardening accelerators. Working mechanisms of known accelerators on silicate hydration are still badly understood. As an example, accelerating early hydration very often results in poor mechanical properties at later ages. This phenomenon is not understood and hence it incites compounders of concrete or developers of new accelerator formulations to find the best compromise in terms of acceleration at the early age and acceptable strength at the mature age. The important mechanisms occurring during the first hours of cement hydration control the whole life of concrete and how it will further evolve after many years.

As a first simplification, it is generally considered that the strength development in cement is obtained by the precipitation of C–S–H. Understanding the C–S–H precipitation, in other words its nucleation and growth, is the key point in order to follow and potentially modify the strength evolution of concrete. Many modeling and experimental works are dedicated to the C–S–H nucleation and growth [1–3]. A model proposed by Garrault et al. [4] was developed to describe C–S–H growth in alite or belite pastes, alite and belite being the principal silicate phases of anhydrous cement. This model allows one to make numerical simulations in order to fit the evolution of alite hydration with time with a small number of fitting parameters. Yet, the fit is possible during the accelerating part of the hydration i.e. only during the very first hours of hydration. These parameters have a clear physical or chemical significance and can be readily varied experimentally. This growth model and the various related numerical simulations on controlled systems have shown good accordance with experimental data, thereby comforting the model validity [5,6]. Such numerical simulations can be helpful in the development of new types of accelerators or to find synergetic combinations between existing accelerator chemistries.

In this study, the aforementioned model was further developed and used to assess the role of various accelerators on the nucleation and growth of calcium silicate hydrate during the hydration of alite. The first step is the validation of simulations, namely it is attempted to correlate simulated output data with experimental data. For this purpose, observations by cryogenic microscopy are carried out in order to estimate C–S–H layer thicknesses formed on alite grains. The measured thicknesses are then compared with the simulated ones. A correlation was also found between the computed permeability of the dense C–S–H layer and the surface density of nuclei.

2. Growth model

Alite hydration is parallel process of dissolution of alite and precipitation of C–S–H with calcium hydroxide:

$$Ca_3SiO_5 + 3H_2O \rightarrow 3Ca^{2+} + 4OH^- + H_2SiO_4^{2-} \quad \text{(alite dissolution)}$$

$$1,7Ca^{2+} + 1,4OH^- + H_2SiO_4^{2-} \rightarrow (CaO)_{1,7}-(SiO_2)-(H_2O)_y \quad \text{(C – S – H precipitation)}$$

$$1,3Ca^{2+} + 2,6OH^- \rightarrow 1,3Ca(OH)_2 \quad \text{(Ca(OH)}_2\text{ precipitation)}$$

The focus of this article is the C–S–H growth. Our study is then limited to alite dissolution and C–S–H precipitation. Recently, it was highlighted that alite dissolution occurs by formation of etch pits [7] as in many other silicate systems already investigated in depth [8–10].

* Tel.: +49 8621862734; fax: +49 862166502734.
E-mail address: luc.nicoleau@basf.com.

0008-8846/$ – see front matter © 2011 Elsevier Ltd. All rights reserved.
doi:10.1016/j.cemconres.2011.04.012

Lasaga postulates and simulates the dissolution of quartz by a step-wave model [11]. Indeed, etch pits can be seen only as the local manifestation of dissolution generated at local crystal defects. In many systems [9,12,13], the global dissolution rate is not dependent of number of etch pits, but only function of solution composition. The grain dissolution can be simply described by the interface retreat. The same framework is used in this study and the alite dissolution is considered as spherically isotropic. The C–S–H precipitation follows a classical nucleation process and is extremely favored onto the alite grains [14]. After nucleation, the growth of each C–S–H crystallite seems to be very limited during the next one-two days; the particle size achieved is always under 100 nm [15,16]. This system prefers to pursue growth by secondary nucleation close to first particles, which has been observed in other systems. Globally, the C–S–H growth on the alite surface can be well described by a precipitation of small particles on and beside the particles already on the surface, as represented on Fig. 1. In order to differentiate this phenomenon from a real crystal growth, the term aggregation will be used in the following as well as the aggregation rate which represents the rate at which C–S–H particles precipitate around other ones.

2.1. Kinetic treatment

During the hydration process when the system has reached a steady state, i.e. when growth dominates nucleation, the hydration rate is equal to the dissolution rate as well as to the precipitation rate:

$$R_{Hyd.} = R_{C_3Sdiss.} = R_{CSHprec.} = -\frac{dN_{C_3S}}{dt} = \frac{dN_{CSH}}{dt} \quad (1)$$

where N_{C3S} and N_{CSH} are the molar quantities of C_3S and C–S–H respectively. The flows of matter brought by the dissolution and consumed by the precipitation have to be equal. It means that the global hydration rate will be limited by the slowest process.

Three different kinetic periods during alite hydration have been already identified in the literature (Fig. 2). The first one occurs at the very beginning of the hydration and can be ascribed to an induction period, often referred and called in the literature the “dormant” period. During this induction period, C–S–H nuclei are created. The second one follows the induction period and corresponds to the free growth of C–S–H clusters, with “free” defined as a lack of steric hindrance to the growth. The hydration rate can be expressed as follows:

$$R_{hyd}(t) = R_{growth}.S_{growth}(t) \quad (2)$$

where R_{growth} is the interfacial anisotropic aggregation rate of C–S–H particles and S_{growth} the surface area of C–S–H clusters. According to the first work of Garrault [4], R_{growth} is kept constant with time. This assumption is sufficient to simulate the very first hours of the hydration. S_{growth} is a non-monotonic function of time, as clusters can collapse on the grain surface after a certain time that leads to a decrease in surface area. Another period step occurs at later times when C–S–H has totally covered alite grains. It was demonstrated that the hydration rate is proportional to the alite surface and to the C–S–H layer thickness [18,19]. At this moment, the hydration is kinetically driven by the dissolution of alite and the subsequent diffusion of dissolved species towards the pore solution. The C–S–H layer formation and the necessary diffusion path up to the pore solution, slows down the dissolution rate and therefore the hydration rate. This means that it will take more time to bring dissolved ions into the pore solution and it will take more time to build a C–S–H particle than at the very beginning when alite surface is still intact. The interfacial growth rate *Rgrowth* defined above and previously fixed constant with time in the work of Garrault has to be reduced over time due to the fact that the dissolution and diffusion affect the delivery rate of ions. These factors are:

1. The decrease of the surface area of alite in contact with water due to decreasing grain size.

This can be easily treated knowing the degree of hydration and the initial grain size distribution. We may express this decrease by $S_{alite}(t)/I_0$. $S_{alite}(t)$ is the surface area of alite grains at time t and I_0 the interface area defined as the alite surface at $t=0$ (Fig. 1).

2. The heterogeneous precipitation of C–S–H on grains.

For this second point, one has to take into account that C–S–H precipitation hinders the free diffusion of ions. In order to reach the bulk, ions have to go through the interface I_0 (Fig. 2). Either they diffuse through the free surface not covered yet by C–S–H particles or they diffuse through the C–S–H layer. The C–S–H layer is comparable to a membrane. Indeed, assuming that the C–S–H layer is constituted of an arrangement of nano-crystallites, it will lead to a nano-porosity. Like a membrane, the diffusion through the C–S–H layer is less rapid and depends on the intrinsic permeability and thickness of the layer. Therefore, the dissolution flow through this membrane is reduced by a transport factor f, f ranges from 0 to 1. The dissolution rates $R(t)$ at instant t and $t=0$ are:

$$R(t) = R_{diss} * \left[I_{free}(t) + \left(I_0 - I_{free}(t)\right)f\right] \quad (3)$$

$$R(0) = R_{diss} * I_0$$

$I_{free}(t)$ is the surface located at the interface I_0 not covered by C–S–H particles and R_{diss} the interfacial dissolution rate. The decrease of the effective dissolution rate over the time may be expressed by the ratio

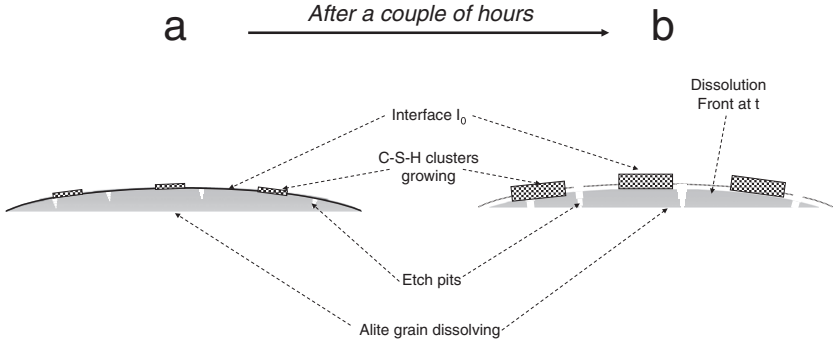

Fig. 1. Schematic representation of C–S–H growth on alite grains at two different times, (a) at the very beginning of hydration shortly after the C–S–H nucleation and (b) a couple of hours after (a). In (b), the alite dissolution front retreated.

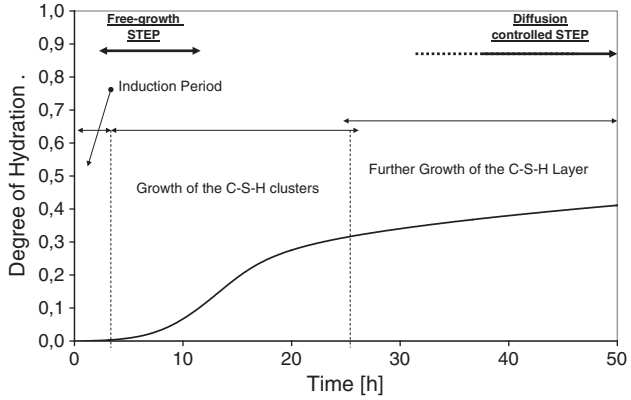

Fig. 2. Example of alite hydration over time (liquid to solid ratio is 0,5). Important phenomena as well as known kinetic steps are noted.

$R(t)/R(0)$. In order to separate effects of intrinsic diffusion change in C–S–H and the layer thickness, we express f as:

$$f = \frac{P}{T(t)} \tag{4}$$

T is the thickness of the C–S–H layer and has the dimension [L]. Therefore, P has a dimension [L] and by analogy is defined as an intrinsic permeability per unit of length. This yields for the hydration rate:

$$R_{hyd}(t) = R_{max} * \left(\frac{I_{free}(t) + \left(I_0 - I_{free}(t)\right) \cdot \frac{P}{T(t)}}{I_0} \cdot \frac{S_{alite}(t)}{I_0} \right) * S_{growth}(t) \tag{5}$$

As defined in the literature [4], R_{max} is the anisotropic interfacial growth rate and depends only on the supersaturation with respect to the C–S–H (the presence of any foreign ions or molecules could also perturb the growth). In [4], the interfacial growth rate is constant with time, this assumption is reasonable since modeling the whole acceleration part of hydration curves was possible. In our case, R_{max} represents the maximal interfacial growth rate when no C–S–H covers the grains surface. The interfacial rates R_{growth} and R_{max} may be expressed in mol $s^{-1} m^{-2}$

Kinetically, the growth rate can be closely simulated by an aggregation of C–S–H particles according to two directions [1,17]. The equation 5 can be applied to experimental data as to the modeling as well. In the modeling, we may compute the anisotropy of the C–S–H growth. In the following, we will consider, as it has been suggested experimentally, that the three-dimensional C–S–H growth rate R_{max} function can be separated in three independent growth rates R_x, R_y and R_z. R_{max} according to the directions x,y,z. R_x,R_y,R_z are linked by the relation $R_{max} = (2*R_x*2*R_y*R_z)^{(1/3)}$ assuming that z is the direction perpendicular to the grain. As explained below, we defined a cubic building unit of C–S–H, this means that the anisotropy of the growth is captured in the difference between rates R_x, R_y and R_z. Another way to proceed could be to define an anisotropic building unit and identical rates.

2.2. Growth simulation on alite grains

Alite is approximated by one sphere. The initial alite grain surface I_0 is mathematically described by an NxN square matrix having n entries ($n = N^2$). $N^2/100$ is the fitting parameter called "alite matrix size". The heterogeneous nucleation is described by a random distribution of primary particles on the anhydrous surface, and mathematically translated by the occupation of certain entries of the matrix by a cubic particle considered as nucleus. This cubic particle is called thereafter C–S–H unit block. The number of these initial cubic particles is the second fitting parameter, which is termed "number of nuclei". The nucleation step is described in the following way in our simulations. The fitting parameter "number of nuclei" is a global number of positions where growth occurs. It may represent therefore the sum of nuclei precipitated during primary and secondary nucleation. Experimentally, we know that the system is always supersaturated with respect to C–S–H. When primary nucleation occurs, even if the growth is thermodynamically favored, C–S–H can possibly further nucleate. First minutes after the primary nucleation, the supersaturation is strongly reduced and C–S–H surface is available, making the nucleation more and more improbable compared to the growth. This time needed to create all nuclei, before that nucleation becomes negligible in comparison to the growth, is defined in the model as an induction time; whereas it is properly not an induction time since it is not correlated with the necessary time to have a critical nucleus.

C–S–H growth is anisotropic as suggested by atomic force microscopy observations [17] and occurs at two different rates, one parallel and one perpendicular to the surface of the grain. Growth is then modeled by a clusterization of blocks around the first ones already put on the matrix. During one single iteration, each cluster on the matrix grows parallel to surface at $2R_x$*$2R_y$ rates and perpendicularly to the surface at the rate R_z until the complete coverage of the matrix. Then, the growth only continues perpendicularly to the surface until the full alite grain consumption. The process is illustrated in Fig. 3. The rates R_x, R_y, and R_z are three fitting parameters in simulations. Despite the fact that there is no direct access to experimental data, we believe that inputs R_x, R_y, and R_z are proportional to the real interfacial growth rates.

The full hydration ($\zeta = 1$) is achieved when $3{,}3.10^8$ blocks have precipitated. The quantity of alite reacting at the beginning is defined by one sphere with a surface $S_{alite}(t=0) = I_0 = N^2$ blocks of CSH. The matrix size $N^2/100$ is the fitting parameter to be input. The increment of time between each iteration is chosen to be 0.833 h. The interfacial rates are defined in block volume per block surface per increment of time, which is equivalent to a block length per unit of time.

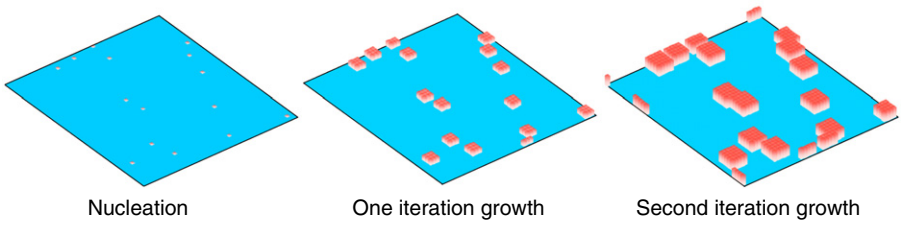

Fig. 3. Schematic representation of the C–S–H growth for 2 iterations. The model is based on anisotropic growth of C–S–H clusters on a grain surface. In this example, the number of nuclei is 15, $R_x = R_y = 3$ and $R_z = 4$.

2.3. Growth simulation on additional substrates

C–S–H can grow heterogeneously not only on C_3S surfaces. It was experimentally observed that C–S–H growth can occur on calcite [20–22], titanium dioxide [23,24], and silica [25,26]. A better description consequently requires that such growth could be simulated. For this purpose, the model was further modified. Namely, a second matrix of growth was created and some nuclei can precipitate on this matrix. These nuclei will grow at the same rates defined in the previous paragraph. That means that the growth simulation on additional surfaces requires only two other fitting parameters which are the additional matrix size (related to the surface area of the material) and the number of C–S–H which nucleate on this surface. This is *a priori* difficult to know. If C–S–H grows on calcite, titanium dioxide or silica, it means that the surface of these materials favor the heterogeneous nucleation of C–S–H. The heterogeneous nucleation of C–S–H on a substrate is the reduction of the barrier energy needed to form a nucleus compared to the homogeneous nucleation. The free energy ΔG needed for heterogeneous nucleation is equal to the product of homogeneous nucleation and a function of the contact angle:

$$\Delta G_{heterogenous} = \Delta G_{\text{homogenous}} f(\theta) \text{ with } f(\theta) = \frac{2-3\ cos(\theta) + cos^3(\theta)}{4} \quad (6)$$

with θ the wetting angle between the nucleus and the substrate, it determines the ease of nucleation by reducing the energy needed to precipitate a critical nucleus. The smaller the wetting angle, the higher the energy decrease, and thereby the smaller the volume of the nucleus V_{het} according to the relation:

$$V_{het} = \frac{\pi . r^3}{3}\left[2-3\ cos\theta + cos^3\theta\right] \quad (7)$$

with r the radius of a critical nucleus. r is a constant for a crystal and only depending on the interfacial crystal-solution energy. The overall quantity of C–S–H nucleating V_{CSH} is proportional to V_{het} by n the number of nuclei:

$$V_{CSH}^{total} = n.V_{het} \quad (8)$$

one rapidly sees that if two materials having the same specific surface area and if V_{CSH} is constant, the material showing the smaller wetting angle will have more nuclei on its surface during the nucleation step. Therefore, we may assume that the smaller the wetting angle, the higher the density of nuclei on the considered substrate. To the best of our current knowledge, only the wetting angle on calcite was determined [14], $\theta_{\text{calcite-CSH}} = 60°$. Nevertheless, as it is demonstrated that CSH can grow also on silica and TiO_2 as references [20–26] referred, we expect that $f(\theta_{silica})$ and $f(\theta_{TiO2}) < 1$.

Even if such a substrate as Calcite is a good substrate for the C–S–H nucleation, it was shown that the alite surface is still more favorable [14]. C–S–H precipitates anyway on alite grains even if the additional material added to the alite is extremely fine. Hence, it seems that the quality of the surface is more important that the quantity. This implies that we cannot compare additional substrates and alite only by their specific surface area but we have also to take into account their capability to reduce the nucleation energy. Secondly, the alite matrix size and the additional matrix size input data reflect both parameters, i.e. the real surface areas occupied by C–S–H after growth. It implies therefore that ratios between matrix sizes on one hand and experimental surface areas on the other hand, are not necessarily proportional.

It is considered here that all additional substrates are inert and therefore their surface area will not evolve during the alite hydration.

3. Experimental section

3.1. Materials

The alite powder was obtained by solid state sintering reactions of freshly decarbonated calcium oxide with fine silica followed by grinding. By Rietveld refinement, it was determined that the powder is composed of 95,5% of a monoclinic polymorph of tricalcium silicate, 4% of dicalcium silicate and 0.5% of free lime. The median diameter of particles obtained by light scattering (MasterSizer 2000 from Malvern Instruments) in ethanol, is 11.75 microns considering the volume size distribution and 4,71 microns considering the surface size distribution. The calculated specific surface area is 0.402 m^2/g.

In this study, four different types of particles were tested as accelerators. Two silica materials were used: Cembinder C50® produced by Eka which is a 15%^{w} suspension of nanosilica having an average particle size of 5 nm, and a fumed silica-1% alumina commercialized by Degussa as Aerosil MOX170 (170 m^2/g and 15 nm average particle size). A fine Portlandite (2 m^2/g and 11 um average particle size) provided by Lhoist was also investigated. Lastly fine calcite, SOCAL®31 provided by Solvay (particle size of approximately 70 nm and a specific surface area of 20 m^2/g) was assessed. Other experiments were carried out with different salts and solutions: calcium chloride, sodium metasilicate pentahydrate, sodium hydroxide, calcium nitrate, and sodium chloride. All these were provided by Aldrich with a purity greater than 99.5%. Finally, a 7% by mass C–S–H suspension commercialized by BASF under the brand X-SEED®100 was also studied.

3.2. Characterization techniques

3.2.1. Calorimetry

3 g of alite and 1.5 g distilled water are mixed manually with a spatula. Then about 1.5 g of paste is added and sealed in a plastic ampoule and inserted in the calorimeter (TAM-AIR, TA Instruments). The temperature is controlled at 20 °C. With this external stirring procedure, one is not able to record the first minutes of reaction and the measurements are slightly perturbed by insertion of the ampoules. Nevertheless the external mixing showed much more reproducible results. The powdered accelerators were first mixed with the alite and the soluble ones were first dissolved in water. The dosages of solid accelerators are indicated in percentage of accelerator solid weight by alite weight and the dosage of salts are indicated in mmol per liter of total water.

3.2.2. Cryogenic microscopy

The Cryo-SEM experiments were performed at Zentrum für Werkstoffanalytik ZWL (Lauf an der Pegnitz, Germany). The mixing procedure for the Cryo-SEM samples preparation is exactly the same as for calorimetry. The different steps realized before observations are accurately described in the following articles [27,28]. This technique presents two huge advantages. First, the paste structure is preserved, and second, it is possible to observe layers around grains. Indeed, due to sample preparation in the pre-chamber, grains are sometime twice cut. If this is the case, cores of anhydrous grains are observed due to the lateral cut, and hydrate growth on the grain surface can be better observed.

4. Results and discussion

4.1. Experimental and simulated curves

Thanks to the heat flows recorded by calorimetry, the hydration degrees of alite over time were calculated. These curves were simulated with the model described in this paper. In Fig. 4, the experimental curves are in plain lines and the corresponding fitted

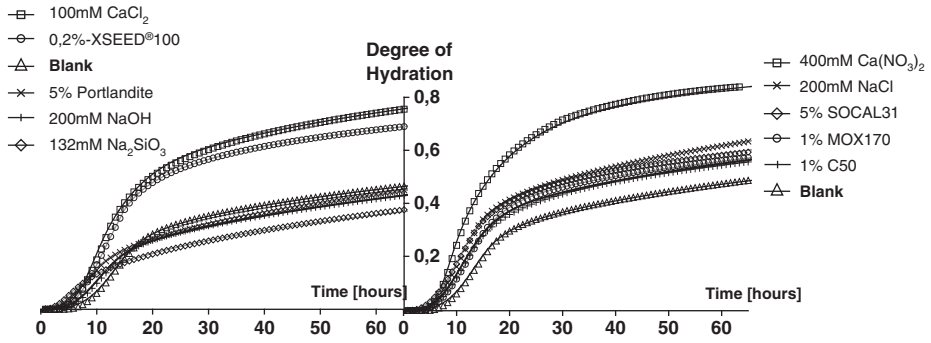

Fig. 4. Experimental (lines) and modeled (symbols) degrees of hydration of alite in presence of accelerators.

Table 1
Fitting parameters describing experimental hydration curves obtained by calorimetry with various accelerators. BL means Block Length, t_i represents the increment time chosen in simulations, for this work $t_i = 0.8333$ h.

	Alite Matrix Size $N^2/100$	Nuclei on alite (blocks)	Rate// [BL]/T_i]	Rate [BL]/T_i]	Introduction Time [Hours]	Permeability P/100[BL]	Additional Matrix Size	Additional Nuclei
Blank	3000	20	6.1	17.2	3.5	1		
5% Portlandite	3000	28	6.5	15.5	0	1.3		
5% SOCAL31{$CaCo_3$}	3000	14	6.1	17	0	0.6	900	8
1% C50 {SiO_2}	3000	15	6.2	16.5	2	0.65	900	9
1% MOX170 Al-rich {SiO_2}	3000	13	6.4	15.5	2	0.52	1180	9
0.2% X-SEED100{SEEDS}	3000	12	6.7	13	2	0.45	3500	28
400 mM CA{NO_3}$_2$	3000	40	5	25	2.5	1.45	2200	30
200 mM $CaCl_2$	3000	33	4.9	25	2	1.4	2500	60
100 mM $CaCl_2$	3000	14	6.8	13	2	0.6	4600	20
132 mM Na_2SiO_3	3000	62	6.9	12.4	0	1.1		
200 mM NaCl	3000	36	5.2	23.5	2	1.45		
200 mM NaOH	3000	22	6.5	15	2	1.1		

curves are represented with symbols. The different parameters of the model are adjusted to obtain an optimum fit to the experimental hydration curves. Nevertheless, alite matrix size, corresponding to the growth area on alite, is kept constant since no modification concerning the quantity or the nature of alite is done. The fitting parameters related to each accelerator tested in this study are gathered in Table 1.

4.2. Model validation

In the past, such simulations based on the original model of Garrault were used in order to investigate deeper the tricalcium silicate hydration in presence of tricalcium aluminate and gypsum [6] or in function of the curing temperature [5]. Both works showed a good concordance between some experimental data and the fitting parameters like the number of nuclei or the specific surface of C–S–H developed during first hours of hydration. More recently, similar simulations have highlighted the possible prediction of the degree of hydration of alite at 28 days obtained by thermal analysis by the fitting of the very early hydration curve obtained by calorimetry [29]. In this article, we aimed to further validate the model of C–S–H growth with an original investigation technique as it is described in the following.

4.3. Correlation between microscopy and modeled C–S–H layer thickness

One of the interesting outputs that can be extracted from these simulations is the development of the C–S–H layer around grains, as seen in Fig. 5. The evolution of the C–S–H layer thickness is of major importance because the interweaving of C–S–H layers hardens cement pastes. In order to get an experimental comparison, layer thicknesses were measured using images collected with cryogenic microscopy in different samples after different hydration times, following the procedure explained in the experimental section. The mean thickness measured for one mixture (paste + water + accelerator), is an average of at least 20 different micrographs observed in three different samples. For each single grain investigated, an average of the layer thickness is made around the whole grain circumference revealed on the micrograph. Some of these micrographs are represented as Fig. 6.

In Fig. 7, all mixes are listed together with their freezing times. One can easily compare how thick the C–S–H layer is and what the model gives accordingly. It can be seen that a linear correlation is obtained between what is measured and what is calculated. This experimental observation technique strongly supports the formation of a C–S–H layer around the alite grains and underlines the validity of the growth model. That allows us to calculate the size length of one C–S–H block, i.e. the slope of the curve in Fig. 5, one CSH cubic block is 2.51 nm long. The surface of alite is covered by $N^2 = 300{,}000$ C–S–H blocks, it

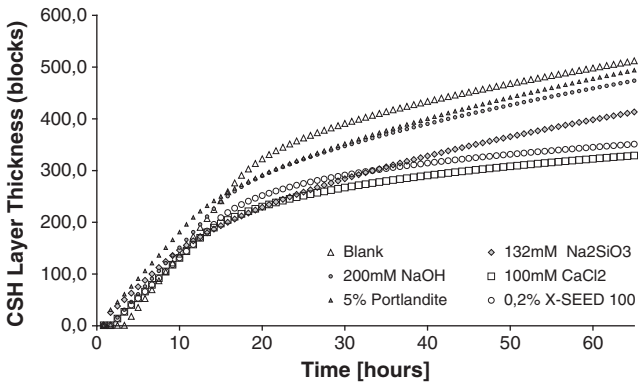

Fig. 5. Simulation of C–S–H layer thicknesses evolution for a subset of accelerators investigated in this study.

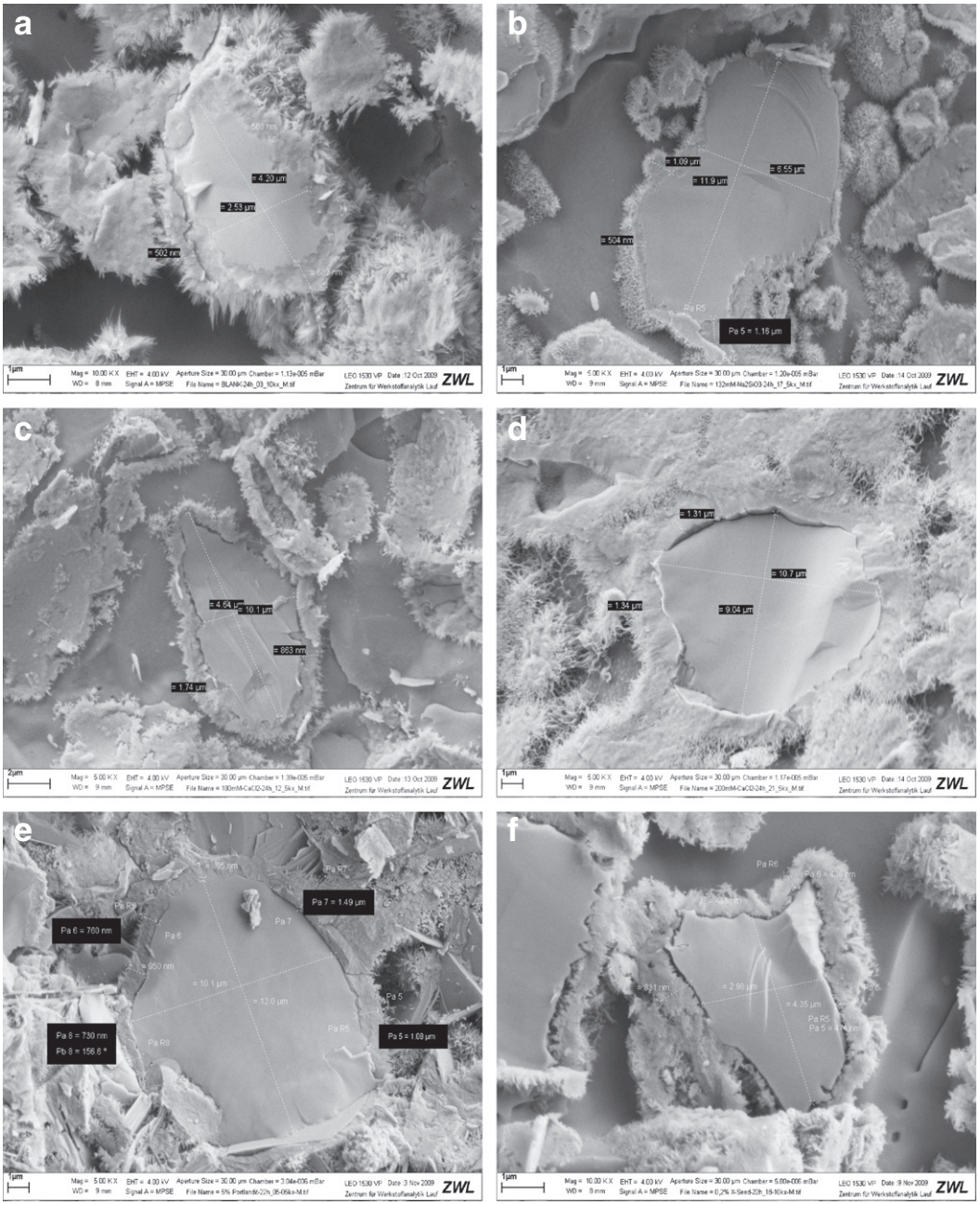

Fig. 6. Cryo-SEM micrographs of alite pastes with and without accelerators. From top left: blank after 24 h (A), with 132 mM Na_2SiO_3 after 24 h (B), with 100 mM $CaCl_2$ after 24 h (C), with 200 mM $CaCl_2$ after 24 h (D), with 5% Portlandite after 65 h (E), and with 0.2% X-SEED after 22 h (F).

corresponds to a surface area of $1.89.10^{-12}m^2$. Considering now the experimental specific area 0.402 m^2/g of the alite sample used in the study with a density of 3.15 g/cm^3, we find out that N^2 corresponds to a sphere with a diameter of 4.47 μm. This is in very good accordance with the surface mean diameter obtained by the grain size analysis (see experimental section, SMD = 4.71 μm).

4.4. Accelerator effects on C–S–H nucleation-growth

Examination of Fig. 4 provides an overview of the accelerating effect of various types of accelerators. Sodium metasilicate, soda and fine Portlandite show higher degrees of hydration only within the first hours, and then a slower compared to the blank. In contrast, calcium chloride and X-SEED®100 accelerate the hydration during at least the first 3 days. Table 1 provides the different fitting parameters which were used to simulate all experimental curves evaluated in this study.

The predominant effect of the Ca-rich powders (Portlandite and calcite) is to completely suppress the induction time necessary to nucleate the first C–S–H. It is interesting to point out that Portlandite, contrary to calcite, does not seem to be a good substrate for C–S–H growth, since it is not necessary to use an additional matrix to simulate the hydration curve. This was confirmed by microscopy, as no C–S–H was found on Portlandite crystals. It also means that the precipitation of Portlandite during alite or belite hydration does not bring any surface for C–S–H nucleation and growth. The Si-rich powders (MOX170 and C50) act as nucleation and growth promoters, since additional surface is required in the simulations. Nevertheless, it can be seen that there are less nuclei on alite. The growth mode is not

Thickness	Calculated (in block)	Measured (in nm)
Blank after 24h	355	933
Blank after 48h	461	1188
132mM Na2SiO3 after 14h	184	427
132mM Na2SiO3 after 24h	253	585
100mM CaCl2 24h	247	601
200mM CaCl2 24h	423	1077
200mM NaOH 26h	326	845
200mM NaOH 60h	459	1183
5% Portlandite after 65h	493	1154
0,2% X-SEED after 22h.	262	722
0,2% X-SEED after 60h	345	819

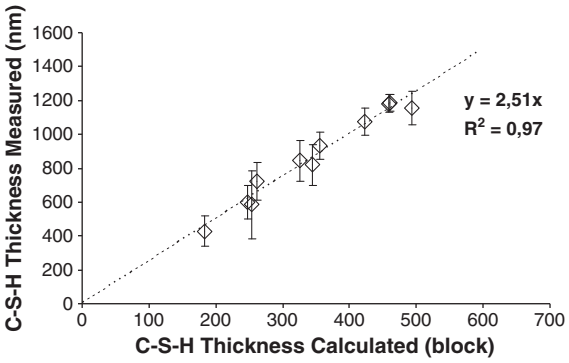

Fig. 7. Comparison between C–S–H layers thicknesses measured and calculated for various mixes and after different hydration times. Error bars represent the standard deviation for each sample.

remarkably changed compared to the reference since the growth rates are almost identical to the reference.

The addition of sodium metasilicate leads to a huge precipitation of C–S–H nuclei which seem to be located on alite grains, which consequently suppresses the induction time. The perpendicular growth rate is decreased. NaCl only slightly promotes the nucleation on alite grains and changes the growth mode. Indeed, the parallel growth rate is reduced and the perpendicular rate increased. The addition of NaOH has almost no effect, except a slight increase of the parallel growth rate and an increase in the number of nuclei on alite, which will lead to a faster coverage of grains by the C–S–H layer.

For other accelerators, namely X-SEED®100 and calcium salts, it is necessary to use an additional matrix of growth to simulate the hydration curves. Actually, there is no reason to think that a substrate is created with these accelerators. Even if one imagines that calcium salts can accelerate the precipitation of Portlandite, it was previously demonstrated that the addition of Portlandite had no effect in this respect. The interpretation of such a result is that instead of heterogeneous nucleation and growth on a substrate, these accelerators allow homogenous nucleation of C–S–H in the pore solution. In this case, the model's additional surface area is a dummy surface which is necessary to reproduce in a way the growth of these homogeneous nuclei in the pore solution. X-SEED®100 supports this idea due to the fact that it is a suspension of C–S–H nano-particles which is homogenously dispersed in the paste and acts as homogenous nuclei [30,31]. With this accelerator, nucleation is moved from grains surface towards pore solution. Although a lot of nuclei are provided, the induction period is reduced but not totally suppressed. The perpendicular growth rate is also notably reduced. Comparing the low dosage of 0,2% for X-SEED®100 and its accelerating performances, it is the most efficient accelerator studied here.

Surprisingly, as previously highlighted, it seems that Ca salts also favor a homogeneous nucleation since we have to add a huge supplementary area to fit experimental curves. The high abundance of Ca ions in the pore solution brought by these accelerators combined with silicate ions dissolved from alite may be an explanation to this phenomenon. In high Ca concentrations, an increase of the perpendicular growth rate is suggested by Garrault [4] and the heterogeneous nucleation on alite grains is also increased. The tendencies observed for calcium nitrate and calcium chloride are very similar. Nevertheless, looking at the dosage, calcium chloride accelerates the alite hydration further.

4.5. Correlation between C–S–H layer permeability and surface nuclei density

In our simulations (Table 1) the phenomena at the origin of permeability variation in dense C–S–H layers are still unexplained and more generally the occurrence of diffusion-limited step is still a subject of debates. Some controversies in the literature exist. Namely people's opinions differ on the fact that the formation of a C–S–H layer on the alite grains may lead to a diffusion-limiting step. In other words, this is still controversial whether the diffusion rate may control the hydration rate or not. Numerical simulations are an ideal tool for investigating if diffusion can affect the hydration rate of alite. With HydratiCa Bullard [2] input the diffusion and introduced a transport factor T_r. This transport factor is a dimensionless coarse-grained parameter used to model the efficacy of ions transport through two types of CSH materials. Indeed, he referred to a dense poorly permeable CSH(I) ($T_r = 0{,}01$) and a less dense high-permeable CSH(II) ($T_r = 0{,}75$). The maximal value of T_r is 1, meaning that the material does not slow down the diffusion compared to the diffusion in water. CSH(I) precipitates in low calcium hydroxide concentration and CSH(II) is high concentration. Experimental curves as well as Bullard's simulated curves typically show that the hydration rate, in the period of time that we define as limited by the diffusion (Fig. 2), is drastically reduced when the hydration leads to exclusively CSH(I) instead CSH(II). In contrast, with the modeling platform μic, Bishnoi [1] attempted to use a diffusion barrier to reproduce the typical drop of the hydration rate for various alite samples with different grain size distributions. He suggested that the broad variation of the fitted diffusion coefficients renders the diffusion-limited kinetic step unlikely.

In order to see the impact of the diffusion on the hydration rate in our simulations, two interesting simulated curves were plotted in Fig. 8. The first one, where $P = 100$, fits perfectly the experimental curve, it corresponds to the hydration of the blank reported in Table 1. In other words, it is assumed that C–S–H material has a defined permeability. For the second simulation, only the permeability coefficient is modified. Here, a fully permeable C–S–H layer is assumed. Hence, there is no limitation of the hydration rate by the diffusion. Yet, the shape of the hydration curve is not drastically changed and the hydration rate still goes through a maximum before decelerating. This decrease is not due to a diffusion process but occurs since the clusters of hydrate begin to coalesce and a hindrance of the free growth appears, as it has been already highlighted by Garrault [4]. The growth extension is reduced which is translated by a decrease of the growth rate. Bishnoi [1] attempted to reproduce this decrease by a diffusion process. This is actually feasible as it demonstrated but it necessitates strong variations of diffusion coefficients within the set of simulations. This diffusion has to slow down the hydration when the rate is the highest. Therefore, this diffusion coefficient must vary with the fineness of alite grains which leads to unacceptable variations for a diffusion coefficient. However, conclusions in Bishnoi's article about the unlikely limitation of the hydration by the diffusion are not necessarily valid since the fitting procedure for the diffusion coefficients do not correspond to a diffusion phenomenon.

From both simulations (Fig. 8), it is possible to extract the effect of the diffusion on the growth rate. Indeed, the ratio between the simulated hydration rates, at the same degree of hydration in the diffusion regime,

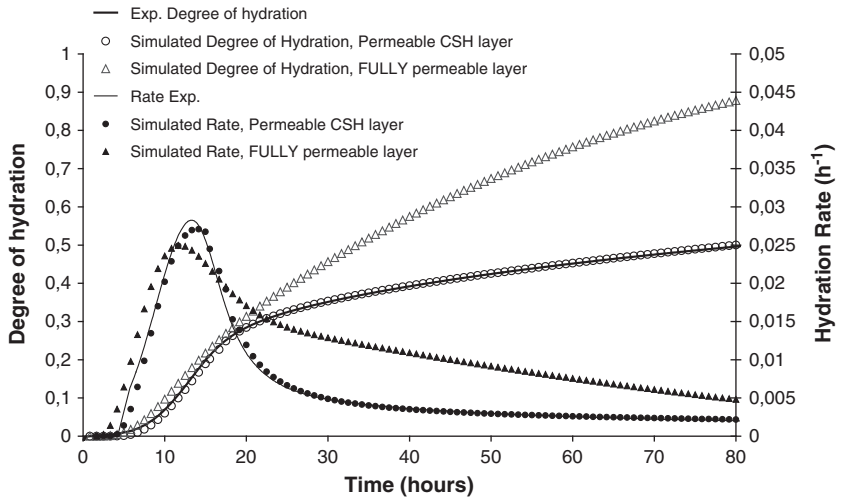

Fig. 8. Experimental (lines) and simulated (circles) curves corresponding to the hydration of the reference mix, the fitting parameters are in Table 1. The other simulated curves (triangles) correspond to the same simulation excepted that the C–S–H layer is considered as fully permeable and no limitation by diffusion can occur. On the right Y-axis are plotted the heat of hydration calculated in our simulations and the experimental heat measured in calorimetry. The heat of hydration is proportional to the hydration rate.

gives us the reduction of the rate due to the slower diffusion through the layer. At a degree of hydration equal to 0,35, reached after about 30 h for the fit with P = 100 (experiment) and after 22.5 h if the CSH layer is fully permeable, the ratio between both hydration rates is 3,2. Coming back to simulations done by Bullard [2] and using his terminology, the effect of the diffusion observed in our simulations corresponds to a transport factor of the layer equal to 1/3,2 = 0,313. This is between the two extreme transport factors Bullard used for CSH(I) and CSH(II). Our observations on the intrinsic C–S–H layer permeability are therefore in good accordance with Bullard's results.

Within the simulation set done in this work, fluctuations of P are observed (Table 1). The C–S–H layer consists of an assemblage of C–S–H particles. The intrinsic permeability P as defined in this article is related to the nano-porosity formed by these latter. Zajac et al. demonstrated experimentally that the hydration rate is connected to the very early nucleation after the layer formation [5]. In this paper, a correlation can also be found between the number of nuclei and the permeability of the C–S–H layer (Fig. 9).

Fig. 9 reveals that the higher the computed nuclei positions, the more permeable the CSH layer will be. This holds up to about 40–50 nuclei positions at which point a decrease in the permeability coefficient occurs. This point, i.e. 62 nuclei positions, represents the simulation done with an addition of sodium metasilicate. Observations from Fig. 9 indicate that nucleation impacts the C–S–H layer permeability, making one think that nucleation topology is important and the arrangement of hydrates can be

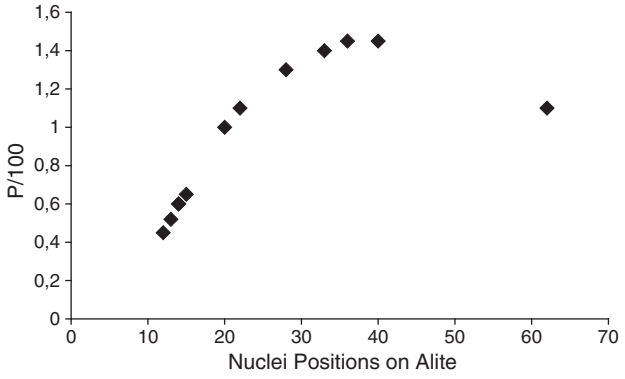

Fig. 9. Relation between the permeability of the C–S–H layer and the number of nuclei coming from fitting parameters in table 1.

at the origin of the layer porosity. The proposed model does not allow for generation of nano-porosity in the C–S–H layer. The layer built in those simulations is uniform, as is the coverage of cement grains by C–S–H. In order to investigate if an equivalent porosity can be created only by an arrangement of C–S–H particles on the surface, a two-dimensional growth of C–S–H clusters was investigated more deeply.

For this purpose, it is assumed that a minimal building block size is required for making particles growing. This means that C–S–H clusters are expanding through the further replication of identical building blocks around the first ones. This is no different than the original model, except for the fact that building blocks are indivisible units and consequently, if there is not a large enough area to put a building block on the matrix, the growth is stopped at this location. Therefore, during the growth of 2D C–S–H clusters, a surface area smaller than one building block between growing clusters remains free. This can be attributed to local porosity. At the end of simulations, when maximal coverage is achieved, no primary particle can be placed onto the surface matrix. An example is given in Fig. 10, where a 100×100 surface was chosen with 5 initial nuclei and a building block size of 5×5. The working hypothesis of such simulations is that the 2D-porosity created by these indivisible building blocks is directly connected to the C–S–H layer intrinsic permeability.

Numerous simulations were run with the matrix size fixed at 100×100, varying the number of nuclei (initial particles) randomly located on the matrix and the building block size. Results are shown in Fig. 10 where the free surface remaining on the matrix at maximum coverage is plotted against (a) the number of nuclei positions and (b) against the surface area of nuclei, for different building block sizes. The surface area of nuclei is the number of nuclei multiplied by the building block size normalized by the total matrix area. For any building block size, the same behavior is observed. The free remaining surface increases with the number of initial nuclei up to a maximum at 30%–35%. At this maximum, there is no growth anymore i.e. the nucleation step is sufficient to maximally cover the matrix. This maximum represents the highest disordered 2D-packing which can be reached by randomly placing all the initial nuclei. After this maximum, if one desires to place more particles, the possible configurations imply that a quantity of nuclei has to be packed close to first ones. Then, the final covered surface stays equal to the surface area of nuclei.

In Fig. 10 (b), curves can be merged in a master curve if the free surface is plotted as a function of the area developed by nuclei normalized by the total area. The fact that a master curve can be

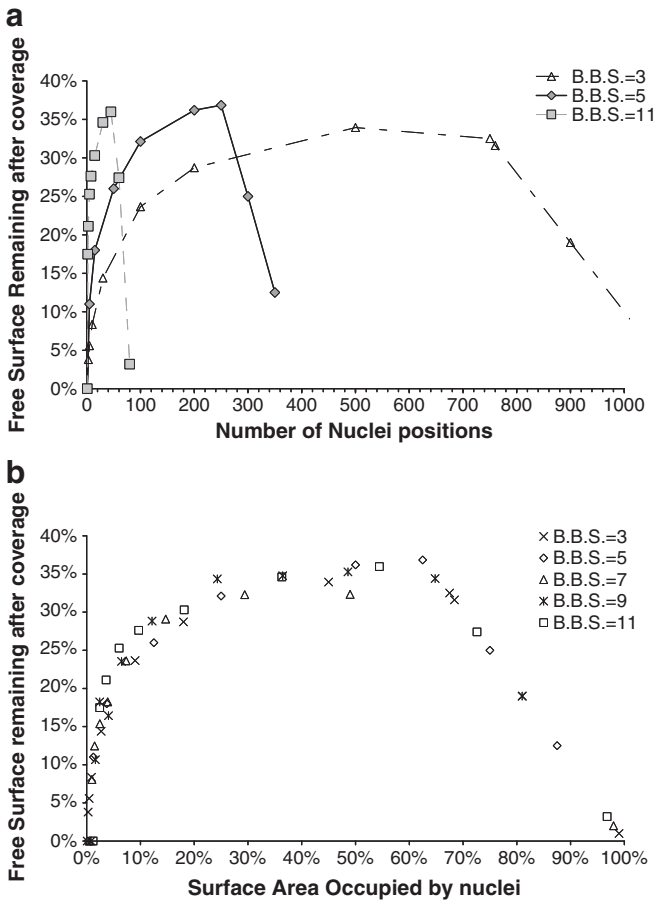

Fig. 10. a & b. Evolution of the free surface remaining after the maximal coverage by some building blocks having different sizes, according to (a) the number of initial positions and (b) the percentage of surface occupied by first building blocks.

obtained reveals that the choice of the building block size do not really matter in our 2D-simulations and that the output porosity has a fractal characteristic. Fig. 11 can consequently be the representation of a 5×5 square micrometer area as well as a 5×5 square nanometer one. This holds as long as only one building block size is used. Assuming that the free remaining surface determines the C–S–H layer permeability, these simulations support the link between the permeability and the arrangement of initial particles. Nevertheless, these 2D-simulations do not perfectly reproduce the behavior observed in Fig. 9. Indeed, the free surface decrease (point at 62 nuclei positions) occurs for a smaller number of nuclei that our simulations can account for. It is important to remember that this point corresponds to the sodium silicate addition that results a huge quantity of silicate in the pore solution. Compared to other accelerators examined in this study, the calcium to silicon ratio in the solution is extremely reduced as well as the calcium to silicon ratio in C–S–H. A shift towards lower calcium to silicon ratios (C/S ratio) implies longer silicate chains [32,33] and we may assume larger building block size than those with other accelerator types. It means that with the addition of sodium silicate, CSH with low C/S ratio should precipitate during the early hydration, followed by CSH with a higher C/S ratio. In the formalism of Bullard, it corresponds to CSH(I) followed by CSH(II) respectively. Unfortunately, our simulation series does not allow for a reasonable variation of the calcium to silicon ratio but it can be suspected that this plays a role on the building block size during the early hydration and therefore on the C–S–H layer permeability. Our 2D simulations demonstrate that the nuclei density has an influence on the porosity of the C–S–H layer.

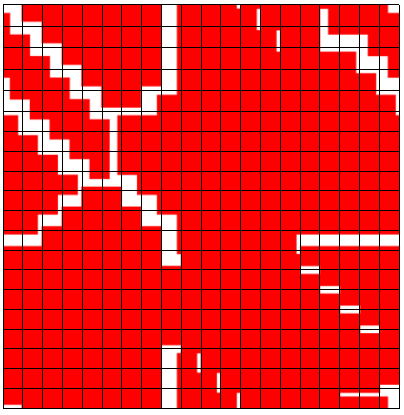

Fig. 11. Matrix 100×100 after maximum coverage obtained by putting 5×5 building blocks. 5 first building blocks were randomly put initially onto the matrix. Red means that the surface is occupied by a building block and white that the surface remains free.

5. Conclusion

It was demonstrated in this study that the model originally developed by Garrault et al. and recently modified allows the modeling of alite hydration and brings precious information about the mechanisms of hardening accelerators on C–S–H nucleation and growth. One of the main results is the possibility to enhance the C–S–H nucleation by a homogeneous precipitation with the use of calcium salts. Furthermore, the model enables us to calculate the C–S–H layer thickness and its development around the alite grains. Cryogenic microscopy measurements were in good accordance with the model. Two-dimensional simulations of the C–S–H growth by replication of finite elements bring some new insights on the origin of permeability variation of C–S–H layer. Further development can be done by accurately calculating the permeability coefficient from other parameters, with experimental knowledge of the C–S–H building block size according to the pore solution composition.

Acknowledgment

The author would like to thank André Nonat for his fruitful discussions and Stephen Farrington for his critical comments which contribute to this article.

References

[1] S. Bishnoi, et al., Studying nucleation and growth kinetics of alite hydration using μic, Cement Concrete Research 39 (2009) 849–860.
[2] J.W. Bullard, A determination of hydration mechanisms for tricalcium silicate using a kinetic cellular automaton model, J. Am. Ceram. Soc. 91 (7) (2008) 2088–2097.
[3] M.M. Costoya, Effect of particle size on the hydration kinetics and microstructural development of tricalcium silicate, Ph-D Thesis N°4102 from E.P.F.L, Lausanne, Switzerland 2008.
[4] S. Garrault, et al., Hydrated layer formation on tricalcium and dicalcium silicate surfaces: experimental study and numerical simulations, Langmuir 17 (2001) 8131–8138.
[5] M. Zajac, Etude des relations entre vitesse d'hydratation, texturation des hydrates et résistance mécanique finale des pâtes et micro-mortiers de ciment Portalnd, Ph-D Thesis from I.C.B., Université of Burgundy, France 2007e.
[6] H. Minard, Etude intégrée des processus d'hydratation, de coagulation, de rigidification et de prise pour un système C_3S-C_3A-sulfates-alcalins, Ph-D Thesis of L.R.R.S., Université of Burgundy, France 2003.
[7] P. Julliand, et al., Dissolution theory applied to the induction period in alite hydration, Cement Concrete Research 40 (2010) 831–844.
[8] O.W. Duckworth, et al., Dissolution rates and pit morphologies of rhomboedral carbonate minerals, American Mineralogist 89 (2004) 554–563.
[9] R.T. Cygan, et al., Dissolution kinetics of experimentally shocked silicate minerals, Chemical Geology 78 (1989) 229–244.

[10] A.C. Lasaga, et al., Variation of crystal dissolution rate based on a dissolution stepwave model, Science 291 (2001) 2400–2404.
[11] A.C. Lasaga, A model for crystal dissolution, Eur. J. Mineral. 15 (2003) 603–615.
[12] A.E. Blum, et al., The effect of dislocation density on the dissolution rate of quartz, Geochimica Cosmochimica Acta 54 (1990) 283–297.
[13] J. Schott, Dissolution kinetics of strained calcite, Geochimica Cosmochimica Acta 53 (1989) 373–382.
[14] S. Garrault-Gauffinet, Experimental investigation of calcium silicate hydrate (C–S–H) Nucleation, J. Crystal Growth 200 (1999) 565–574.
[15] S. Gauffinet, et al., AFM **et** SEM studies of C–S–H growth on C3S surface during its early hydration, Proceedings of the international Conference on Cement Microscopy, 1998, pp. 337–356.
[16] B. Möser, Nano-Charakterisierung von Hydratationsvorgängen mittels hochauflösenden REM-Abbildungstechniken, Proceedings of the 16th Internationale Baustofftagung, 2006, pp. 1–0347-1-0366.
[17] S. Gauffinet, et al., Sur l'aggrégation em 3D des C–S–H, C.R, Acad. Sci. Ser. IIa 327 (1998) 231–236.
[18] S. Garrault, et al., Formation of the C–S–H layer during early hydration of tricalcium silictae grains with different sizes, J. Phys. Chem. B 110 (2006) 270–275.
[19] Lecoq X., Etude de l'hydratation à concentration contrôlée du silicate tricalcique Ca3SiO5 et des caractéristiques de ses produits de réaction, Ph-D thesis of L.R.S.S. (1993), University of Burgundy.
[20] S. Ruffing, et al., Microsctructural studies on hydration of tricalcium silicate with calcite, Proceedings of the 20th GDCh-Monographie, 2002, pp. 172–176.
[21] J. Pera, et al., Influence of finely ground limestone on cement hydration, Cement Concrete Composites 21 (1999) 99–105.
[22] B. Lothenbach, et al., Influence of limestone on the hydration of Portland cements, Cement Concrete Research 38 (2008) 848–860.
[23] Lee B.Y. et al., Influence of TiO2 nanoparticles on early C3S hydration, ACI Special publication (2009), 267 SP, 35–44.
[24] W.A. Gutteridge, et al., Filler cement: The effect of the secondary component on the hydration of Portland cement: Part I. A fine non-hydraulic filler, Cement Concrete Research 20 (5) (1990) 778–782.
[25] A. Korpa, et al., Hydration behaviour, structure and morphology of hydration phases in advanced cement-based systems containing nanoscale pozzolanic additives, Cement Concrete Research 38 (2008) 955–962.
[26] J. Zelic, et al., The role of silica fume in the kinetics and mechanisms during the early stage of cement hydration, Cement Concrete Research 30 (2000) 1655–1662cbe.
[27] Poellmann, et al., Combination of Cryo-SEM, in-situ XRD and heat-flow calorimetry for early time hydration studies of Portland cements, Proceedings of the International Conference on Cement Microscopy, 2008.
[28] M. Fylak, et al., Electron microscopic studies of hydration reactions of Portland cements by Quantomix-test substrate and cryotransfer preparation, Proceedings of the GDCh-Monographie, 2006, p. 36, Tagung Bauchemie.
[29] A. Nonat, et al., Tricalcium silicate hydration modeling and numerical simulations, Proceedings of Conmod, 10, 2010, pp. 91–94.
[30] L. Nicoleau, New calcium-silicate-hydrates network, Proceedings of 1st conference of Nanotechnology in Cement. Transportation Research Record, 2010.
[31] J.J. Thomas, et al., Influence of nucleation seeding on the hydration mechanisms of tricalcium silicate and cement, J. Phys. Chem. C 113 (11) (2009) 4327–4334.
[32] D. Damidot, et al., C3S hydration in diluted and stirred suspensions: (III). NMR study of C–S–H precipitated during the two kinetic steps, Advances Cement Research 7 (25) (1995) 1–8.
[33] X. Cong, 29Si MAS NMR Study of the structure of calcium silicate hydrate, Advances Cement Based Materials 3 (1996) 144–156.